Magnetic Fabric Analyses of Basin Inversion: A Sandbox Modelling Approach

Thorben Schöfisch[1], Hemin Koyi[1,2], Bjarne Almqvist[1]

[1]Hans Ramberg Tectonic Laboratory, Department of Earth Sciences, Uppsala University, Uppsala, 75236, Sweden
[2]Currently at: Department of Earth Sciences, Khalifa University of Science and Technology, Abu Dhabi, 127788, United Arab Emirates

Correspondence to: Thorben Schöfisch (thorben.schofisch@geo.uu.se)

Abstract.

Magnetic-fabric analysis is a useful tool to display deformation in nature and in models. In this study, three sandbox models represent basin inversion above a velocity discontinuity (base-plate). After complete deformation of each model, samples were taken in different parts of the models (along faults and areas away from faults) for magnetic fabric analysis. Model I, which simulates basin formation during extension, shows two kinds of magnetic fabric: an undeformed/initial fabric in areas away from faults, and a normal fault-induced fabric with a magnetic foliation that tends to align with the fault surface. Models II and III were extended to the same stage as Model I, but were subsequently shortened/inverted by 1.5 cm (Model II) and 4 cm (Model III). Both inverted models ~~which were initially extended before they were shortened,~~ developed thrusts ~~faults~~ during inversion. The thrusts show an alignment of magnetic foliation parallel to the fault surfaces that depends on the maturity of the thrust. Our results highlight that thrusting is more efficient in aligning the magnetic fabric along them compared to normal faults. Moreover, models II and III reveal a magnetic fabric overprint towards a penetrative strain-induced fabric (magnetic lineation perpendicular to shortening direction) with increasing strain in areas away from thrusts ~~faults~~. Such overprint shows a gradual transition of a magnetic fabric to a penetrative strain-induced fabric and further ~~towards~~ into a thrust-induced fabric during shortening/inversion. In contrast, extension (Model I) developed distinct magnetic fabrics without gradual overprint. In addition, pre-existing normal faults are also overprinted to a penetrative strain-induced fabric during model inversion. They define weak zones within the main pop-up imbricate and steepen during model inversion. Steepening influences the magnetic fabric at the faults, and, in general, the strain propagation through the model during inversion.

The magnetic fabric extracted from the models presented here reflect the different stages of basin development and inversion. This study is a first attempt of applying magnetic-fabric analyses on models simulating inverted basins. ~~However, the~~ This study illustrates the possibility of applying a robust tool, i.e., magnetic-fabric analyses, to sandbox models, whose initial, intermediate, and final stages are well documented, to understand fabric development in inverted tectonic regimes.

Graphical Abstract.

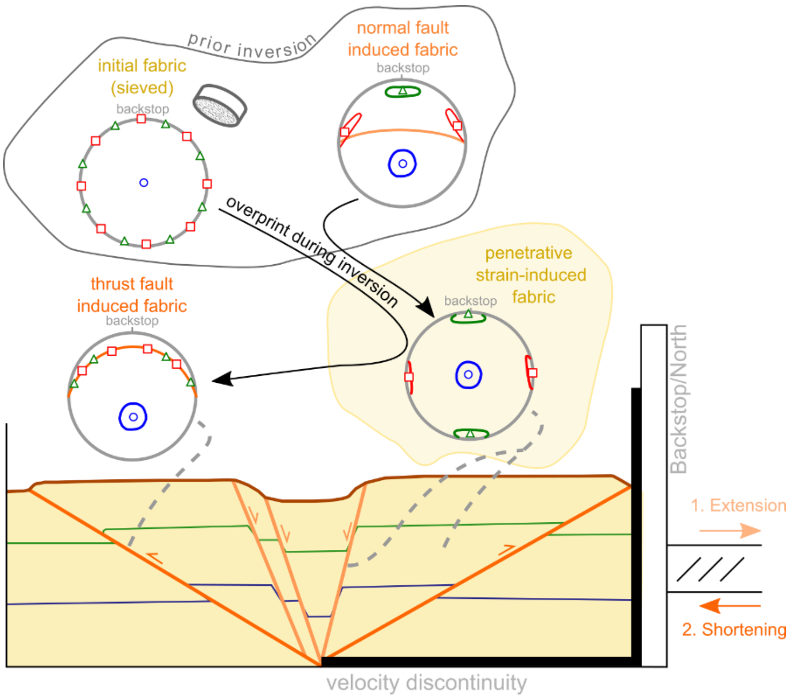

1 Introduction

Anisotropy of magnetic susceptibility (AMS or magnetic fabric) is a useful strain indicator in analogue models simulating compressional tectonic regimes (García-Lasanta et al., 2017; Almqvist and Koyi, 2018; Schöfisch et al., 2020; Schöfisch et al., 2022). AMS measurements provide information about the bulk orientation of the magnetized grains within a collected sample. From the AMS measurements, a magnetic susceptibility ellipsoid with three principal axes of susceptibility ($k_{max} \geq k_{int} \geq k_{min}$) is described. Analyses of the susceptibility ellipsoid is similar to the strain ellipsoid, and changes of the magnetic ellipsoid can be related to strain changes (e.g., Hrouda and Janák, 1976; Jelinek, 1981; Kligfield et al., 1981; Hrouda, 1982; Hirt et al., 1988; Borradaile 1988, 1991; Borradaile and Henry, 1997; Bakhtari et al., 1998; Parés, 1999; Parés and van der Pluijm, 2002; Borradaile and Jackson, 2004; Burmeister et al., 2009; Parés, 2015).

Several publications summarize the magnetic fabric development of basin and ~~its~~ basin inversion derived from analyses of natural examples (e.g., Sagnotti et al., 1994; Mattei et al., 1997, 1999; Cifelli et al., 2005; Soto et al., 2007, 2008, 2012, 2016; Oliva-Urcia et al., 2010, 2013, 2016; García-Lasanta et al., 2014, 2015, 2018; Marcén et al., 2019; Burgin et al., 2021). Relating the magnetic fabric observed in extensional settings reveals an overprint of a sedimentary fabric by an extension-related fabric, which shows a magnetic lineation (k_{max} axes clustering) parallel to extension (Sagnotti et al., 1994; Mattei et al., 1997; Borradaile and Hamilton, 2004; Cifelli et al., 2005). With the development of normal faults, the magnetic lineation develops parallel (i.e., a shear-related fabric) or perpendicular to the transport direction (i.e., as intersection fabric) ~~(i.e., a shear-related fabric)~~ along the fault surface (Marcén et al., 2019) ~~or perpendicular to the faults (Cifelli et al., 2005)~~. Extensional magnetic fabrics can be preserved during basin inversion when either shortening is not significant enough or thrust development accommodates shortening and a passive displacement of the basin prevents overprinting of the magnetic fabric. Where magnetic fabric is overprinted during inversion, the development of the magnetic fabric depends on the inversion style (García-Lasanta et al., 2018). According to observations by Averbuch et al. (1992), Bakhtari et al. (1998), Parés et al. (1999), and Parés and van der Pluijm (2002), the magnetic fabric (i.e., magnetic foliation defined by a girdle distribution of k_{max} and k_{int} axes) becomes parallel to the developed tectonic foliation. Also, a magnetic lineation develops parallel to an intersection lineation that later changes into a stretching lineation with increasing deformation.

The effect of overprinting of an existing "sedimentary" magnetic fabric by a tectonic fabric is supported by results of analogue sandbox models (Almqvist and Koyi, 2018; Schöfisch et al., 2020; Schöfisch et al., 2022). Even though the effects of grain deformation, ~~fluidal movement~~fluid flow or recrystallization (i.e., changes in magnetic mineralogy and development of sub-fabric) on development of magnetic fabric ~~development~~ in crustal tectonic settings are not represented in sandbox models simulating upper crustal deformation, analogue modelling highlights the importance of grain reorientation during deformation (e.g., Schöfisch et al., 2022). The non-cohesive granular material used in sandbox experiments accommodates deformation by grain rotation, and hence change/initiation of magnetic fabric which can be investigated in order to better understand fabric evolution in natural prototypes.

The current ~~is~~ study evaluates the potential of AMS as a strain gauge in sandbox models simulating the development of basin and basin inversion. Furthermore, ~~this~~ the study aims to understand the development of magnetic fabric in extensional settings and its overprint during basin inversion.

2 Methods

2.1 Experimental Setup

2.1.1 Model Preparation

For this study, three models (I, II, III) were prepared with a similar base plate setup (Fig. 1) at room temperature (22°C and humidity of 50-60%). Models were initially 8.3 cm thick, 30 cm wide and 40 cm long. A basal metal plate was attached to the moveable backstop that created a velocity discontinuity in the middle of the model (20 cm from the backstop) beneath the layers of sand-magnetite mixture (Fig. 1). The sand-magnetite mixture was used to simulate the brittle behaviour of sedimentary rocks in the upper crust and consist of loose sand and magnetite (< 0.1 vol%), both with similar subangular shape and grain size (0.124-0.356 mm). The average of bulk susceptibility of the sand-magnetite mixture is 1.9 x 10^{-3} [SI]. This indicates that ~~T~~the artificial high content of ferromagnetic multi-domain magnetite in the models (compared to natural examples) governs the bulk signal of the AMS and the influence of the diamagnetic sand can effectively be neglected. Single layers of sand-magnetite mixture were carefully sieved from a height ranging between 30-50 cm above the model. The layers, which were sieved to ~~had~~ varying thicknesses (0.9-1.5 cm) due to manual sieving ~~by hand~~, were separated by ~~a~~ thin layers of coloured sand acting as passive markers. The rationale behind sieving the sand-magnetite granular mixture into the sandbox and accepting irregularities in layer thickness throughout the model was to avoid scraping, which has proven to create~~s~~ an artificial initial magnetic ~~lineation as an initial magnetic~~ fabric (e.g., Schöfisch et al., 2022). The uppermost layer of each model consisted of sand only and was scraped after sieving to create an even model surface with same model height for all three models. ~~Note that t~~No samples were taken from this uppermost layer for ~~was not used in the~~ AMS analysis. On the surface of the models, coffee powder was sieved as well as point markers (coloured sand) were set for monitoring surface deformation. Monitoring surface deformation is used for comparing the models and their development, but are less crucial for the outcome of this study. -The sidewalls of the sandbox model were transparent glass walls that allowed monitoring the model evolution during extension and inversion from the sides.

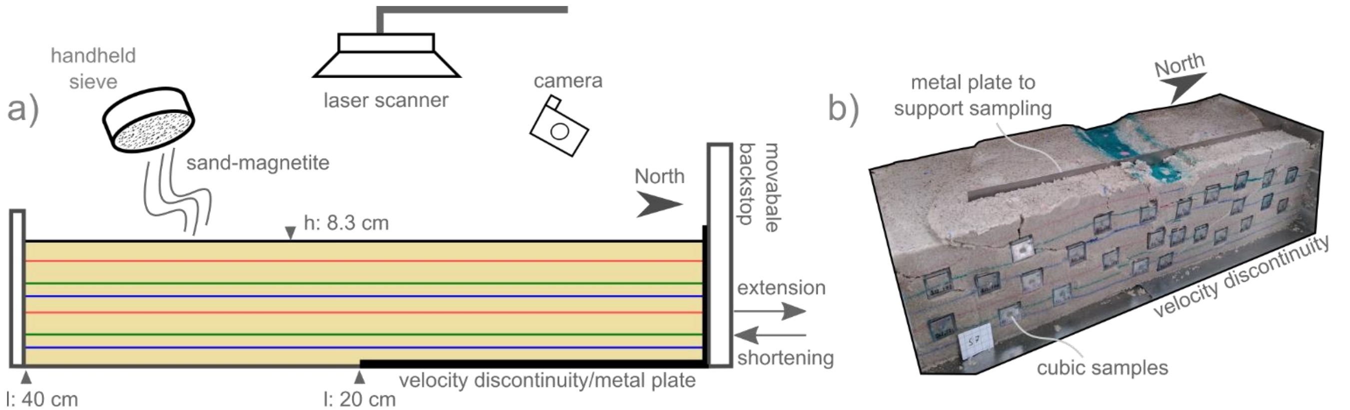

Figure 1: (a) Sketch of model setup. Sieved layers of sand-magnetite mixture are separated by coloured sand layers. A basal metal plate was used as velocity discontinuity and attached to the backstop that moved backwards for extension and forwards for shortening the model. The models were monitored by taking pictures from different angles with camera and model surfaces were monitored by laser scanning during deformation. (b) Photo of section number 7, which is an oblique view of Model III with inserted sample cubes, showing the procedure of sampling of the models.

2.1.2 Model Run, Sectioning, and Sampling

All three models (I, II, III), which were identical in setup, were extended up to 1 cm in total. However, only models II and III were inverted. During extension, the model runs were paused after 0.5 cm of extension to fill the developed basin. After the extension phase, models II and III were shortened by different amounts of bulk shortening to simulate basin inversion at different stages. Extension and shortening of the models were initiated by a constant moving backstop with a velocity of 3 cm/hr, to which a velocity discontinuity was attached. To describe orientation clearly, the backstop of the model was labelled geographic model north~~ for orientation~~. ~~-~~Model I simulated extension only. Model II was shortened by 1.5 cm after extension and stopped when first kinks developed (i.e., when sand layers ~~were~~ showed amillimetres offset ~~by millimetres~~ monitored through the transparent sidewalls of the sandbox), before any thrust ~~fault~~ forms with larger displacement. Model III was shortened by 4 cm after the initial ~~1 cm~~ extension. This 4 cm amount of shortening represents the stage, when the backthrust of Model III showed a similar amount of displacement as the pre-existing normal fault. Moreover, the differences in the amount of bulk shortening between the models II and III allows a comparison of i) magnetic fabric of inverted basins with that of extensional stage, i.e., prior to shortening, ii) basin development and inversion with same amount of bulk extension and shortening, and iii) magnetic fabric at normal faults and thrusts ~~faults~~ with similar displacement.

During deformation, the models were monitored by a series of photos from all ~~sites~~sides. After final stage of deformation, models were carefully wetted for vertical sectioning parallel to the extension and shortening direction, as well as for allowing model sampling for AMS analysis (Fig. 1b). ~~During the sampling, oriented plastic cubes (internal volume 1.7 cm^3) were carefully pressed horizontally into the model.~~ Each section was taken individually and had a width of 2-2.5 cm~~ wide~~. Before sampling a section, the next section was prepared and ~~cut and~~ a stable plate was placed between the two sections. This stable plate ~~to~~ supported sampling of the outer section ~~(i.e., pressing the cube into the cohesive sand-magnetite with stable support from the other side~~ without exerting pressure on the rest of the model (i.e., where the next section would be taken, see Fig. 1b). During the sampling of a section, oriented plastic cubes (internal volume 1.7 cm^3) were carefully pressed horizontally into the cohesive material. Afterwards, ~~T~~the cohesive and wetted AMS samples were stored in semidry conditions (fridge with 7°C and humidity of 75%), allowing for AMS measurements over a few weeks before the material inside the plastic cube lost ~~loses its~~ cohesion.

In total, 721 samples (Model I: 217, Model II: 241, Model III: 263) were taken across the models targeting the different structures. The focus of sampling was to acquire magnetic fabrics of different parts of the models (e.g., normal faults, thrusts, graben, footwalls, hangingwall-~~imbricates~~blocks). This exercise eliminated the effect of measuring a bulk mixed AMS fabric, which may be created due to a small structure-to-sample-size ratio. However, it is not possible to entirely diminish this effect at faults. Sampling at faults covers the narrow fault zone and the vicinity of a fault. The vicinity of a fault might have a different magnetic fabric than observed directly at a fault plane. Consequently, a mixed fabric is represented by the bulk measurement of samples from fault zones. Such an effect needs to be considered during magnetic fabric interpretation of fault-associated datasets. Therefore, a structure-to-sample-size ratio is calculated (see Fig. S1 in Supplement~~ary Material~~).

2.1.3 AMS Measurement and Analysis

The bulk susceptibility and magnitude of AMS samples was measured with a MFK1-FA Kappabridge (Agico Inc.) in a low-field (976 Hz) with an AC field strength of 200 A/m at room temperature. The grains within a sample respond to an applied external magnetic field, and the directional variation of the "response" (magnetic susceptibility) is described through a symmetric second-rank tensor with six independent matrix elements. The eigenvalues and eigenvectors of the matrix are the principal axes of susceptibility ($k_{max} \geq k_{int} \geq k_{min}$) that describe the magnitude, orientation, and shape of a magnetic susceptibility ellipsoid. The maximum axis (k_{max}) describes the magnetic lineation, whereas the plane containing the maximum and intermediate axes (k_{max} and k_{int}) describes the magnetic foliation. Orientation of the principal axes were plotted in ~~an~~ equal-area lower hemisphere projections with north assigned towards the backstop of the model and the primitive circle (outer circle of projection) being parallel to the initial horizontal layering/bedding. The corrected degree of anisotropy, Pj,

$$Pj = exp\sqrt{\{2[(n_{max} - n_{mean})^2 + (n_{int} - n_{mean})^2 + (n_{min} - n_{mean})^2]\}} \quad (1)$$

with $n_{max} = \ln(k_{max})$, $n_{int} = \ln(k_{int})$, and $n_{min} = \ln(k_{min})$~~)~~ reveals information about the sorting of grains within a sample, where a high degree of anisotropy corresponds to a preferred alignment of grains, whereas a low degree of anisotropy indicates a variation of grain orientations (Hrouda, 1982). Additionally, the shape of the susceptibility ellipsoid is described by T,

$$T = \frac{2\, n_{int} - n_{max} - n_{min}}{n_{max} - n_{min}} \quad (2)$$

where $T = 1$ represents an oblate shape, $T = 0$ is neutral triaxial shape, and $T = -1$ is a rotational prolate shape. The principal axes, the corrected degree of anisotropy (Pj), or the shape of anisotropy (T) were statistically interpreted and visualized with the help of graphical tools, MATLAB, and ArcGIS. The centre of each AMS sample defined the distance to a fault or the model surface (i.e., depth). Samples that were not perfectly located with their centres on a fault were still assigned to the fault-induced AMS dataset. Therefore, we introduced a threshold with a range of 0.8 cm (centre to corner of a sample) between their centre to a fault. Samples located within this threshold were labelled to be fault-induced.

2.1.4 Uncertainty in AMS Measurements

~~Furthermore, i~~In section view, the area of a sample was compared to the area of the fault zone, and a sample-size-to-structure ratio is calculated (Fig. S1 in Supplement~~ary Material~~). This ratio allows specifying the amount of AMS signal induced by a fault relative to that induced by the ~~non-~~unfaulted area within the sample. Moreover, this ratio can explain a broad scattering in the magnetic foliation (i.e., girdle distribution of k_{max} and k_{int} axes) from data collected along the faults (Fig. S2 in Supplement).

Further uncertainties in the AMS datasets can be related to the sampling procedure, sample handling during measurements, and the instrument itself. The signal sensitivity of the instrument is 2×10^{-8} [SI], which is well below the signal of samples in this study. Using a relatively high content of ferromagnetic minerals produces a clear signal with narrow confidence ellipses and high F-values (see dataset in Schöfisch, 2021). The F-values provide information about the anisotropy of the measured material, and show a relation between measured principal susceptibility axes and measurement errors (Jelinek, 1977). Confidence ellipses and measurement errors are not shown in the figures, as the symbols in the figures would overlap the uncertainty estimated from measurements. Additional variations in orientation in the principal axes can derive from sampling or by adjusting the samples in the instrument. In both cases, the sample can deviate from alignment with the reference/modelling north. However, the large amount of data from the different areas across the models provide a basis for statistical analysis and average out outliers in the dataset. Further scattering in the datasets/figures are addressed in the Discussion section. Note that interpretations of the magnetic fabric within the grabens are limited to the small number of samples and no solid statistical interpretation can be taken for internal graben changes.

3 Results

3.1 Model I: Basin formation (extension only)

Model I developed an east-west striking graben ~~structure~~ bounded by two normal faults that dip 60-70° ~~towards each other~~ (Fig. 2). The ~~south-dipping normal fault (~~northern fault (~~/~~Normal Fault B) shows a displacement of ~1.4 cm. With progressive extension, a couple of synthetic and antithetic faults form in the ~~hanging-wall~~center of the graben (Fig. 2). AMS analysis of different parts of this model reveals that there is no sign of deformation in the footwalls on either side of the graben; ~~it~~ they only show~~s~~ the oblate initial fabric ~~that is~~ produced by sieving, with k_{min} axes clustering vertical, as the pole ~~of~~ to bedding, and k_{int} and k_{max} axes spread in the horizontal plane along a primitive circle (Fig. 2). The ~~magnetic fabric~~ principal axes in Footwall

B ~~is~~ show more scattered orientation and have wider confidence ellipses (Fig. 2 and Fig. S3 in Supplement) ~~and~~. However, they display ~~has~~ a ~~lower~~ comparable distribution in degree of anisotropy similar to that ~~compared to the magnetic fabric~~ observed in Footwall A (Fig. 3b). Within the graben, the magnetic fabric is similar to the fabric observed in the footwalls and shows the initial fabric (Fig. 2). ~~However~~Along the normal faults, ~~the magnetic fabric along the normal faults differ from the initial fabric as k_{min} axis is rotated away from its vertical orientation, and~~ k_{max} and k_{int} axes ~~have~~ form~~ed~~ a sub-horizontal (10-20°) magnetic foliation ~~(Fig. 2)~~ with the same dip direction as that of the normal faults; dipping north along normal faults A and south along normal fault B (Fig. 2). However, the magnetic foliation and inclination of the normal faults are oblique to each other (~50°). The k_{min} axes display rotation away from its vertical position into the opposite direction of the fault dip, as it is perpendicular to the magnetic foliation ~~The rotation direction of k_{min} axis is determined by the dip direction of the normal fault; the k_{min} axis rotated in the opposite direction of the fault dip. However, generally, there is a tendency of the magnetic foliation to align parallel to the fault surface~~ (Fig. 2). Moreover, the magnetic fabric is mostly oblate, but the degree of anisotropy is on average lower along the normal faults (1.14 < Pj < 1.40) compared to the fabric in the graben ~~(hanging wall)~~ and its footwalls (1.15 < Pj < 1.51) (Fig. 3a, and ~~d~~c).

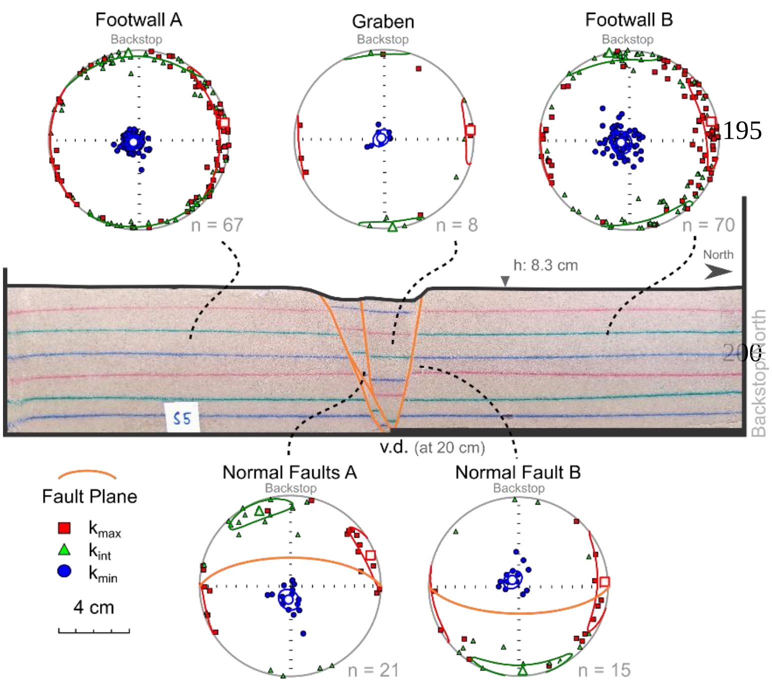

Figure 2: Representative section of Model I shows a graben that is bounded by normal faults (orange lines). The magnetic fabric for each structure/area is plotted on equal-area lower hemisphere projections with the confidence ellipses and mean of each principal axis.

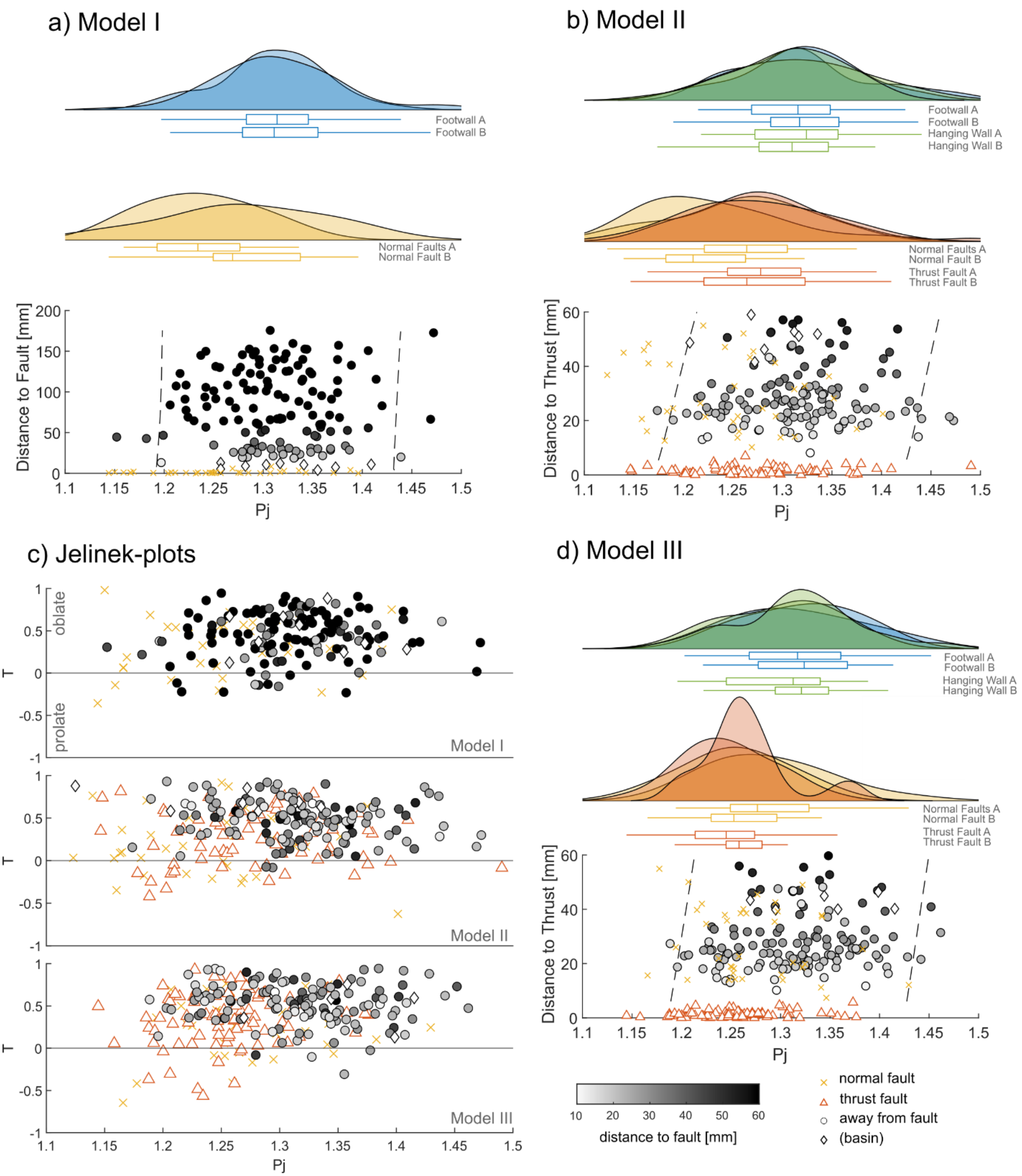

Figure 3: Distribution of degree of anisotropy (Pj) is plotted as density distribution for each structure against the distance to the closest normal fault /or thrust (a,b,c) for (a) Model I, (b) Model II, and (d) Model III. (c) Jelinek plots (degree of anisotropy Pj and against the shape of anisotropy (T) (d,e,f) for each model. Note, the greyscale colormap of (a,b,c) is defined by the distance towards the closest normal fault, whereas the colormap of (d,e,f) is defined by the distance to the closest thrust fault.. The dashed lines shows

the 95%-confidence interval of the data away from the faults. The figure is using a modified MATLAB script of a raincloud plot by Allen et al. (2021).

3.2 Model II: Basin Inversion

The second model (Model II) was extended 1 cm before it was ~~and~~ later shortened 1.5 cm (V1 in Supplement). Similar to Model I, an east-west striking graben developed during the extension phase (Fig. 4). With the onset of subsequent shortening (i.e., beginning of inversion) of the model, the normal faults steepened by ~2-3°, which led to a slight narrowing of the graben (Fig. S1 in Supplement~~ary~~). The final dip of the normal faults in this shortened model is steeper (70-85°) than that of the normal faults of Model I which underwent only an extension phase. However, the normal faults did not display any significant ~~reactivation~~inversion, during the subsequent shortening. Instead, precursors of gently-dipping thrusts ~~faults~~ (25-35°) developed as kinks, which offset footwall markers by a few millimetres. These "thrusts~~ faults~~" are less mature than the normal faults as they developed less displacement. The thrusts divided footwalls A and B of the graben (Fig. 2) into footwalls and hanging walls (Fig. 4). Moreover, hanging walls A and B of the graben developed to a large pop-up structure (including the graben structure) that was uplifted along the thrusts during inversion. For comparison of the magnetic fabric and its development in the different areas, we labelled the different blocks based on their relation to the thrust faults (Footwall A, Hanging wall A, etc.).

The magnetic fabric~~s~~ of footwalls A and B, as well as of the hanging wall-blocks A and B show an oblate magnetic fabric that is similar to the initial fabric with~~(~~ vertical k_{min} axis, and horizontal spread of k_{max} and k_{int} axes~~)~~ (Fig. 4). It is noted that the k_{max} distribution creates a subtle magnetic lineation parallel to the east-west axis in these areas away from the faults and that the confidence ellipses are narrower compared to the same areas in Model I. Furthermore, there is no clear distinction between the degree of anisotropy between the footwall (1.19 < Pj < 1.48) and hanging wall areas (1.17 < Pj < 1.45) of Model II (Fig. 3b). Additionally, the central graben reveals similar magnetic fabric as those in footwall~~s~~ and hangingwall-blocks~~-imbricates~~ (Fig. 4). The magnetic fabric~~s~~ at the normal faults A and B display a ~~scatter~~ distribution of subvertical k_{min} axes. The mean of the subvertical k_{min} axes are tilted opposite to the dip direction of the normal fault and points steeply to the south for Normal Faults A and to the north for Normal Fault B. The k_{max} and k_{int} axes are mostly plunging ~~oriented subhorizontally~~gently (< 30°) with a dominant east-west orientation for k_{max} axes and north-south for k_{int} axes (Fig. 4). The principal axes are similarly clustered at the normal faults of Model II compared to Model I, in particular for the k_{max} orientations. However, the plane created by k_{max} and k_{min} axes (i.e., magnetic foliation) shows little to no inclination with regards to ~~Magnetic foliation along the normal fault surface is less pronounced than~~ that along the normal faults in Model I. AMS data from the thrusts ~~faults~~ in Model II show a similar distribution of principal axes ~~distribution~~ as the normal faults (Fig. 4). However, the k_{max} and k_{int} axes for each thrust ~~fault~~ tend to define a magnetic foliation subparallel to the thrusts~~ faults~~. In Model II, the magnetic fabric along both the normal faults and the thrusts ~~faults~~ is mainly oblate with some occurrences of prolate shape (Fig. 3c). The degree of anisotropy is comparable between the normal faults (1.12 < Pj < 1.38) and thrusts ~~faults~~(1.14 < Pj < 1.41), but it is on average lower than in areas away from the faults (Fig. 3b).

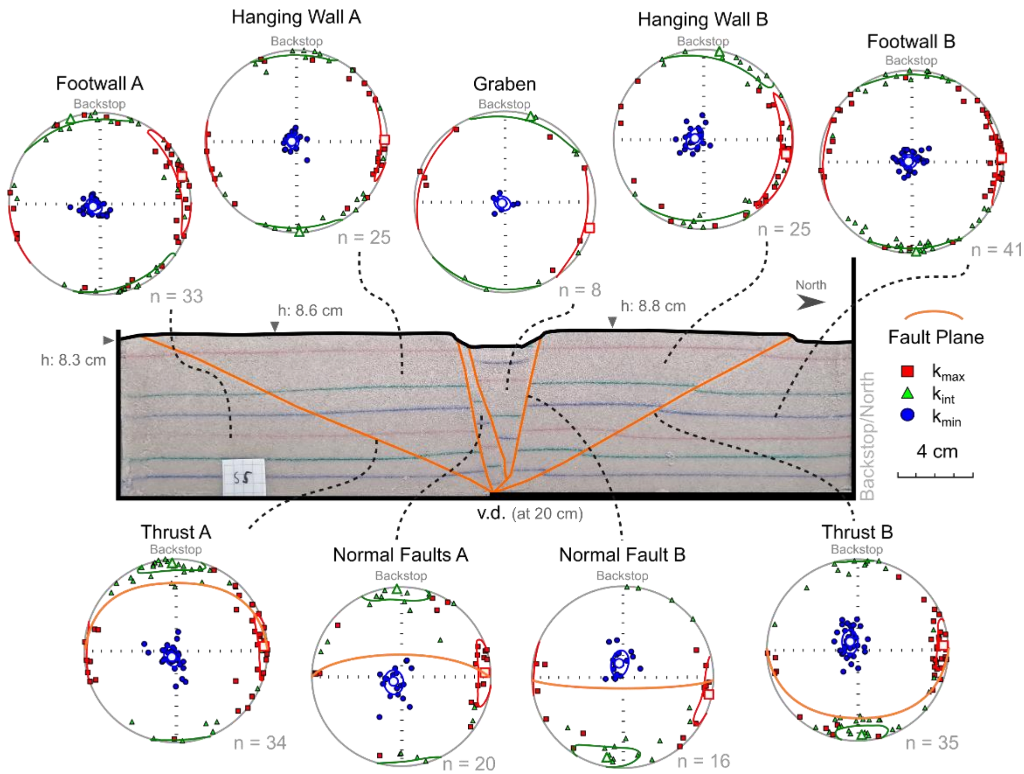

Figure 4: Representative section of Model II ~~with its developed~~showing extensional and compressional structures. The ~~associated~~ magnetic fabric of each structure/area ~~are~~ is plotted on equal-area lower hemisphere projections with confidence ellipses and mean of each principal axis.

3.3 Model III: Inverted Basin Model (advanced shortening)

Model III shows similar structures to those in Model II (V2 in Supplement). However, the thrusts ~~faults~~ in Model III, which was subjected to larger amount of bulk shortening (+2.5~~3~~ cm more than Model II), are more mature and display larger displacement than those in Model II (Fig. 5). The normal faults dip 70-80° and show a displacement of ~1.4 cm o~~i~~n average. During inversion, Normal Fault B steepened by ~5°, whereas Normal Faults A maintained ~~remain with~~ the same dip as that prior to shortening (Fig. S1 in Supplement~~ary~~). Similar to Model II, with subsequent shortening of Model III, the pre-existing graben narrowed with rotation of the normal faults by few degrees (Fig. S1 in Supplement~~ary~~). Moreover, Hanging Wall A shows a minor block rotation (~10°) along Thrust A during the development of the main pop-up structure, which involves folding of the layers in the vicinity of the thrust. ~~The~~ Both thrusts ~~faults~~ dip in a range between 25-40° ~~and~~. However, Thrust A developed a splay at deeper parts of the model and shows less displacement than Thrust B due to a different accommodation of strain in this area (Fig. 5). Thrust B shows a displacement of ~1.4 cm, which is similar to that along the normal faults. ~~Additionally, the southern thrusts (i.e., Thrust Fault A) splays in the deeper parts of the model (Fig. 5).~~ Similar to Model II, we divided and labelled the different blocks of Model III individually based on their relation to the thrusts (Footwall A, Hanging wall A, etc.).

In Model III, the magnetic fabric in footwalls A and B, the hangingwall-blocks ~~imbricates~~ A and B, and the graben ~~are developed~~ similar ~~to the initial fabric, which is also similar to the~~ magnetic fabrics as those observed ~~from~~ in equivalent areas of the other two models (i.e., Models I and II). However, there are minor deviations from the initial fabric in certain areas, in particular when comparing the clustering of the principal axes and their confidence ellipses. For example, Hanging Wall A developed a slight tilt in the magnetic foliation plane (~10°) that corresponds with the slight rotation of bedding during uplift of this block (Fig. 5). Furthermore, ~~I~~in footwalls A and ~~Footwall~~ B, and in Hanging Wall B, the k_{max} axes are clustering horizontally (i.e., creating a magnetic lineation) along east or west directions instead of spreading around the primitive circle. Furthermore, k_{int} axes also cluster mainly in a north and/or south direction (Figs. 5 and 6). ~~Clustering of k_{max} and k_{int} axes in the Footwall B is different from that in Footwall A, graben, and hangingwall-imbricates, where k_{max} and k_{int} axes are spread around the primitive circle. (Fig. 5).~~

The principal axes (k_{max}, k_{int}, and k_{min} axes) distribution along the normal faults in Model III is comparable to that along the normal faults of Model II (Fig. ~~5~~6). The cluster of k_{min} axes (i.e., mean of k_{min} axes orientations) rotates slightly away from its vertical orientation to subvertical orientation, dipping south for the north-dipping Normal Faults A and dipping north for the south-dipping Normal Fault B. AMS analysis does not show a clear girdle distribution of k_{max} and k_{int} axes (i.e., magnetic foliation) parallel to the normal faults ~~surfaces~~. Instead, k_{max} and k_{int} axes are more clustered than the axes in models I and II (i.e., less stretched confidence ellipses), and the plane described by both axes (i.e., magnetic foliation) is almost not inclined at Normal Faults A and slightly inclined (~10°) at Normal Fault B (Figs. 5 and 6). However, k_{max} axes cluster horizontally towards the East or West (i.e., perpendicular to the extension and shortening directions), whereas k_{int} axes distribute along a North to South axis (i.e., parallel to extension and shortening directions). ~~Nevertheless, along Normal Fault A, the magnetic foliation tends to be sub-parallel to the fault surface~~). Moreover, the magnetic foliation has similar orientation as the fault surfaces themselves, although both planes are oblique (50-60°) to each other (Fig. 5). In contrast, the magnetic foliation is parallel to the thrust ~~fault~~ in Model III. Even though displacement along the thrusts ~~faults~~ is comparable to that along the normal faults ~~of the model~~, the magnetic foliation associated with thrusting is distinct (*cf.* Schöfisch et al., 2022). The degree of anisotropy of the normal faults (1.16 < Pj < 1.43) is distributed ~~similar~~similarly to that of the thrusts ~~faults~~ (1.14 < Pj < 1.38) (Fig. 3d). ~~with similar distribution of the~~ The shape of anisotropy along the normal faults and thrusts~~, which mainly~~ plots mainly in the oblate field with some degree of prolate signature (Fig. 3c). The degree and shape of anisotropy along the structures in Model III are similar to that in the other two models (Fig. 3c). Moreover, the degree of anisotropy along the faults is on average lower than that observed in the footwalls (1.2 < Pj < 1.46) and hanging walls (1.18 < Pj < 1.47) (Fig. 3d).

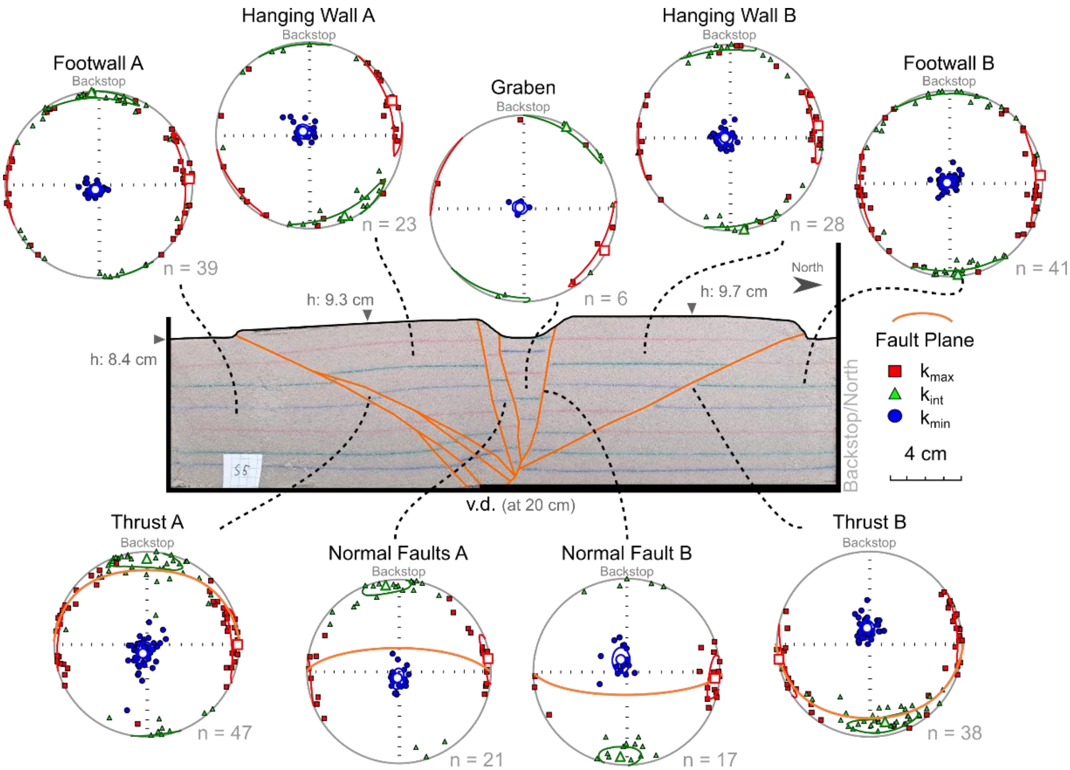

Figure 5: Representative section of Model III ~~with its developed~~ showing the main structures, and corresponding magnetic fabric plots. ~~The associated magnetic fabric of each structure/area are plotted on equal-area lower hemisphere projections with confidence ellipses and mean of each principal axis.~~

4 Discussion

4.1 Initial magnetic fabric

The initial fabric of the models was created by sieving, where k_{min} axes cluster as the pole to bedding, and k_{max} and k_{int} axes orient randomly in the horizontal plane parallel to bedding. This initial fabric is the reference and changes from this initial fabric are attributed to deformation. Sieving the initial magnetic fabric is a novelty, tested in this study~~, and introduced in sandbox models simulating compressional tectonic regimes (Schöfisch et al., in prep)~~. The sieved fabric differs from the scraped fabric; a scraped initial fabric shows horizontal alignments of k_{max} axes parallel and k_{int} perpendicular to the scraping direction (Almqvist and Koyi, 2018, Schöfisch et al., 2020; 2022), whereas k_{max} and k_{int} axes in a sieved magnetic fabric distribute randomly in different horizontal directions. Such a sieved magnetic fabric is similar to a sedimentary fabric that is observed in nature (*cf.* Borradaile and Henry, 1997; Bakhtari et al., 1998; Parés et al., 1999) and allows an improved interpretation and comparison between models and natural prototypes (e.g., Figs. 6 and S3 in Supplement)~~analogies (Schöfisch et al., in prep)~~.

The footwalls A and B of Model ~~I~~I ~~a~~re undeformed and reveal still the initial fabric after extension. It can be noted that the magnetic fabric in Footwall B of Model I has a relatively larger scatter compared to Footwall A of the same model (Figs. 2 and S3 in Supplement). Footwall B is resting and carried on the basal plate that moves during extension, whereas Hanging wall A is resting on a stationary base. ~~and w~~We assume that the deviation in magnetic fabric is due to grain reorientation/bulk compaction of sand due to vibration during movement of the underlying plate. An "undeformed" pile of sand is more prone to vibration as a pile that is under compression. Therefore, we assume that an influence of a vibration is more obvious during the phase of extension compared to shortening. The slight vibration could be because of a minor gap between the table and the metal plate. However, the weight of the model above the plate was removing this gap, but still, such gap could be an explanation for a potential source of vibration. The modelling setup was reworked during preparation of models II and III and the gap between table and metal plate was removed. Models II and III also retain the initial fabric in some locations even after model inversion, but both models also developed a clustering of principal axes with narrower confidence ellipses that is attributed to penetrative strain (Fig. 6). Consequently, the magnetic fabric in models II and III away from faults represent a mixed fabric between the initial and penetrative strain-induced fabric. ~~these~~ These locations with initial fabric in models II and III indicate undeformed areas. Such undeformed areas during basin development are also known from natural examples (Oliv~~i~~a-Urcia et al., 2013; Garcí~~i~~a-~~-~~Lasanta et al., 2018).

4.2 Extensional fabric in basin model

In a natural sedimentary basin, a magnetic lineation (i.e., k_{max} clustering) develops parallel to the axis of extension. This observation derives from studying the reorientation of phyllosilicates in clay-rich sediments (e.g.; Mattei et al., 1997; 1999; Cifelli et al., 2005). However, the surface markers of the models of this study indicate movement of the individual developed hanging- and footwall (i.e., graben and Footwall B) without noticeable internal deformation (i.e., stretching) of the lithology during extension of the models. The magnetic fabric within the hanging wall and footwall of Model I has not developed a clear magnetic lineation parallel to stretching (Figs. 2 and Fig. S3 in Supplement). ~~and~~ It rather indicates localized deformation, where the normal faults are developed (Fig. 2). The lack of pervasive extensional fabric in the model is likely a consequence of the granular material used in the model that has very low cohesion (cf. Eisenstadt and Withjack, 1995; Eisenstadt and Sims, 2005). ~~Consequently~~However, our results underscore that there is minimal to no layer-parallel deformation/extension within the different hanging- and footwalls during extension in such brittle deformation environment (i.e., using a ridged velocity discontinuity/basal plate for initiating deformation).

The normal faults of Model I show a magnetic foliation that vaguely align parallel to the fault surface (note: normal faults of models II and III are discussed in section 4.3.2). However, this alignment is ~~weak~~ oblique and there is a large difference of ~40-50° between the inclinations of magnetic foliation and of the fault surface (Figs. 2 and 6). Nevertheless, the dip direction of the magnetic foliation and fault surface are identical. Dilation is involved in the formation of normal faults in granular material. Dilation on one hand forms a weak zone that is important during later basin inversion, but on the other hand it is responsible for developing the observed magnetic fabric at the normal fault. The subangular non-cohesive grains rotate with their k_{max} axis along the normal faults into a clustering in east or west direction that is parallel to the fault plane but perpendicular to the direction of model extension. The clustering is also reflected by the lower degree of anisotropy that is observed at the normal faults compared to the rest of Model I, where initial fabric dominates (Fig. 3a). The lower degree of anisotropy reflects a greater alignment of the magnetic grains at the normal faults compared to the grains away from the faults. However, the described oblate magnetic ellipsoid is not aligned with the fault surface (Fig. 3c), as the k_{int} axes and, in general, the magnetic foliation is oblique to the fault plane (Figs. 2 and 6). It can be interpreted that the grains are sliding along the fault and rotate, with a tendency of being tilted along dip direction of the fault but not being aligned completely with the fault surface.

Overall, the magnetic fabric of the normal faults differs ~~to the initial fabric, especially,~~ in ~~the~~ degree of anisotropy and clustering of principal axes to the initial fabric that is observed ~~is generally lower at normal faults compared~~ ~~to~~ at the rest of the model~~, which mainly show the initial fabric~~. These differences in magnetic fabric in Model I are results of extensional deformation. Although, there is no presence of a layer-parallel extensional fabric, an "extensional fault-induced fabric" (i.e., normal fault-induced fabric) developed in Model I as consequence of localized deformation during basin development.

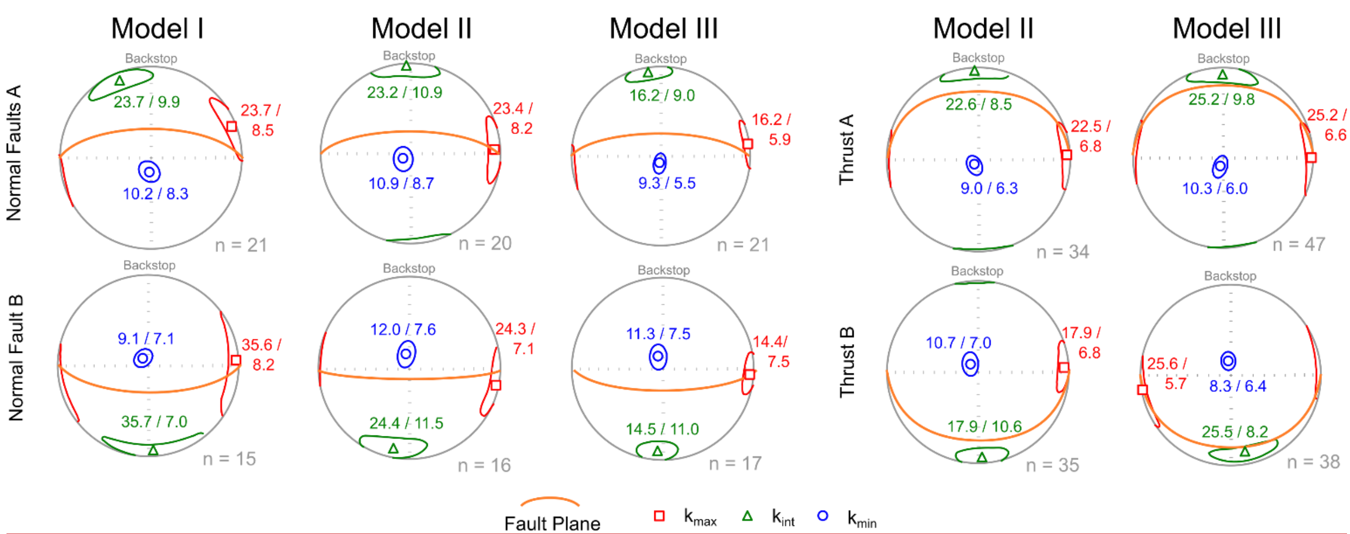

Figure 6: Comparison of orientation of the mean principal axes with confidence ellipses for normal faults and thrusts. The numbers next to each confidence ellipse are the angles of the ellipse itself, which give information of the length and width of the ellipse in degrees (Jelinek, 1977). A comparison of the areas away from the faults is given in the Supplement S3.

4.3 Overprint of magnetic fabric in models during inversion

4.3.1 Thrust overprint

Models II and III simulate basin inversion at different stages. Model II developed kinks along the thrust surfaces that offset the layers by a few millimetres, whereas Model III developed more mature thrusts that offset the layers in the model by the same amount as the pre-existing normal faults (Figs. 4, and 5). It has been reported that compaction and folding (i.e., kinking) takes place prior to thrusting (e.g., Mulugeta and Koyi, 1992; Koyi, 1995; Koyi et al., 2003). The different thrusts in the models follow the same deformation path and reveal a magnetic fabric that is associated with their development. Model I shows an initial fabric at the same location/area where the thrusts developed in models II and III. The kinks in Model II developed a magnetic lineation (i.e., cluster of k_{max} axes) towards the east and west, which is perpendicular to the shortening direction. Such orientation is also related to penetrative strain as it represents a penetrative strain-induced fabric. Moreover, the confidence ellipses of the k_{max} and k_{int} axes define a magnetic foliation that is slightly tilted. This tilt is attributed to the onset of kinking and development of a thrust. With further evolution of a thrust, the confidence ellipses are stretching and defining a magnetic foliation that aligns with the thrust surface (Fig. 6). Meanwhile, the degree of anisotropy is decreasing with increasing displacement along a thrust (Fig. 3), which indicates a better sorting and greater alignment of the grains. Thrust B in Model III shows such alignment of magnetic foliation with the thrust surface, whereas Thrust A in the same model diverges slightly from such alignment. This difference in alignment can be related to the structural complexity and structure-to-sample size ratio, where Thrust B is a well-defined single thrust, whereas Thrust A represents a splayed fault system. However, ~~Therefore,~~ the development of the thrust-induced fabric in the models ~~of this study~~ follows a similar evolution of fabric development ~~(from initial fabric via a penetrative strain-induced fabric towards the thrust-induced fabric)~~ as observed in a recent study by Schöfisch et al. (2022); the initial fabric is first overprinted by penetrative strain before thrusting aligns the magnetic foliation parallel to the fault surface. Moreover, Schöfisch et al. (2022) related the alignment of magnetic foliation parallel to the thrust surface with maturity of a thrust. Similar observations are made in the current models; magnetic foliation shows a closer alignment with thrusts of Model III than with the thrust surfaces (i.e., kinks) in Model II (Fig. 6).

The overprint of magnetic fabric during thrusting differs ~~to/~~from ~~the overprint~~that observed ~~at~~ along the normal faults. The alignment of fabric to the thrust surfaces is displayed by k_{max} and k_{int} axes defining a broad girdle distribution (i.e., magnetic foliation) parallel to the thrust surface. In contrast, t~~T~~he normal faults ~~- show also a broad scatter (referring to Model I, whereas normal faults in models II and III show an additional overprint during inversion; discussed in section 4.3.2). The broad scatter~~

~~in this girdle distribution seems to be an artefact of sampling and the related structure-to-sample-size ratio (Fig. S2 in Supplementary). However, such artefact cannot be the reason for a large discrepancy between magnetic foliation and fault geometry at the normal faults in the models.~~ developed a magnetic foliation oblique to its fault surface. Comparing the magnetic fabric ~~from~~ along the normal faults to that along the thrusts~~,~~ with ~~the~~ similar displacement along the fault surface (~~Figs.2, 3, and 4~~Fig. 6), it is apparent that thrusting is more efficient in aligning grains parallel to a fault.

4.3.2 Magnetic fabric overprint at normal faults

Normal faults of ~~the~~ models II and III show no or very minor reactivation during inversion, which is in agreement with observations of pure-dry-sand models by Eisenstadt and Sims (2005) and Deng et al. (2019). However, the grabens ~~of~~ in models II and III become narrower during inversion and the normal faults rotate slightly to steeper angles (Fig. S1 in Supplement~~ary~~). Such basin narrowing and fault rotation are consequences of the development of the main pop-up imbricate that is bounded by the thrusts in models II and III. As penetrative strain ~~compaction~~ precedes thrusting, the sand package, including the graben and normal faults, experiences layer-parallel shortening. Similar to what has been reported in previous studies (cf. Eisenstadt and Withjack, 1995; Bonini et al., 2012, Deng et al., 2019), this layer-parallel shortening reworks the pre-existing extensional structures and the associated grain alignment without reverse displacement along the faults. The magnetic fabrics at the normal faults of models II and III are rearranged from a normal fault-induced fabric towards a penetrative strain-induced fabric during subsequent inversion/shortening of the models. In more detail, the overprinted normal faults of models II and III show a clustering of k_{max} axes to the East and the West, and of k_{int} axes to the North and the South (Fig~~s. 4, and 5, and.~~ 6). The clustering of k_{max} and k_{int} axes is classified as penetrative strain-induced fabric that becomes more distinct (narrowing of confidence ellipses) with higher bulk shortening (~~comparing the normal faults in models II and III~~ in Fig. 6). This clustering in magnetic fabric differs from the k_{max} and k_{int} axes distribution with elongated confidence ellipses of the normal faults in Model I. Additionally, the magnetic foliation rotates towards the horizontal, which is parallel to the direction of model shortening (Fig. 6). In conclusion, the normal faults are ~~less~~not kinematically reactivated (i.e., no inversion ~~) in the sense of kinematics~~, but ~~rather~~ show an overprint towards a penetrative strain-induced fabric that is accompanied by geometrical change of the fault during superimposed shortening. ~~withsubsequent inversion.~~

4.3.3 Penetrative strain distribution during inversion

With the onset of model shortening (i.e., inversion), the models II and III were horizontally compacted before the thrusts developed. The models accommodated the penetrative strain by grain rearrangement, which is reflected by the change in magnetic fabric. Early signs of basin inversion in nature have been reported to be recognized by the reorientation and development of magnetic lineation perpendicular to shortening direction in a basin (e.g., De Lamotte et al., 2002; Soto et al., 2016). Such development of magnetic lineation perpendicular to shortening direction can be observed in the models II and III; k_{max} axes cluster horizontally along an east-west axis (penetrative strain-induced fabric) in the areas away from the thrusts

(Figs. 4, 5, and Fig. S3 in Supplement). For example, Footwall B of models II and III shows a narrowing of the confidence ellipses and east-west magnetic lineation, which is more pronounced compared to the same area in Model I (Fig. S3 in Supplement). With increasing strain, other areas, such as the hanging walls, also show a magnetic fabric change towards a penetrative strain-induced fabric. However, depicting deviations of the initial fabric in the models and referring this to penetrative strain, especially, when rotation and clustering of a magnetic lineation are parallel to bedding, needs careful interpretation. Some k_{max} orientations differ from the penetrative strain-induced fabric within the footwalls and hanging wall-blocks~~imbricates~~ of the models. This means a mixture is ~~monitored~~ detected between a penetrative strain-induced fabric (k_{max} cluster/magnetic lineation perpendicular to the shortening direction) and the initial fabric (k_{max} axes spread around the primitive circle) in these areas away from thrusts (Figs. 4, and 5). It is common that the initial fabric prevails in some locations even after basin inversion in nature (Oliv~~i~~a-Urcia et al., 2013) and in sandbox models simulating shortening only (Schöfisch et al., 2022). An observation of a mixture between initial fabric and penetrative strain-induced fabric, or a prevailing initial fabric after deformation, indicate~~s~~ that penetrative strain is heterogeneously distributed within the model and further, deformation within single block ~~imbricates d~~ (hanging wall/ footwall) ~~eform internally~~occurs heterogeneously.

Heterogenous penetration of strain within the model occur due to accommodation of strain during inversion by pre-existing structures like normal faults (cf. Sassi et al., 1993; Eisenstadt and Withjack, 1995; Bonini et al., 2012~~,~~; Tong et al. 2014). The pre-existing normal faults create weak zones within the main pop-up structure, which develops during inversion. These weak zones accommodate most of the penetrative strain within the pop-up imbricate during model inversion and therefore, deform internally, as seen by the geometric reorientation of the normal faults. Normal faults in models II and III develop a magnetic lineation during inversion that is similar to the magnetic fabric induced by layer-parallel shortening (k_{max} axes cluster perpendicular to shortening direction) (see discussion 4.3.2). Consequently, the normal faults accommodate strain, and the geometric change of the normal faults are signs of internal, penetrative deformation within a pop-up imbricate during inversion. Strain accommodation ~~Such accommodation of strain~~ by pre-exiting faults contribute to a heterogenous internal deformation and consequently ~~that,~~ results in a mixed magnetic fabric within ~~both~~ the footwalls and hanging walls.

4.3.4 Gradient in magnetic fabric with increasing bulk shortening

Shortening in the models is driven by the backstop and the velocity discontinuity from one direction (i.e., from the model North). Therefore, areas closer to the backstop and velocity discontinuity compact before deformation penetrates farther into the model (Mulugeta and Koyi, 1992; Koyi, 1995). This is seen by a clear and distinct magnetic lineation (i.e., a penetrative strain-induced fabric) in Footwall B of ~~Model~~ models II and III, which is the footwall next to the backstop. Areas farther from the backstop (e.g., Footwall A and hanging~~-~~wall~~- imbricates~~ blocks of Model III) are also affected by penetrative strain, but, show a mixture between a penetrative strain-induced fabric and the initial fabric (as discussed earlier in 4.3.3). Nevertheless, there is a gradient in clustering of principal axis with increasing bulk shortening. When Model II shows a clear penetrative strain-induced fabric in Footwall B and partially in the hanging walls, Model III shows a narrowing of the confidence ellipses in almost all areas of the model (Fig. S3 in Supplement). Consequently, it could be argued that there is a general gradient in amount of penetrative strain from model~~ling~~ north to model~~ling~~ south in the inverted models. However, such general gradient is not linear, because strain is also increasing with decreasing distance towards a thrust within thrust imbricates (Fig. 3) (cf. Schöfisch et al., 2022).

The magnetic fabric changes with increasing strain (e.g., Borradaile and Henry, 1997; Bakhtari et al., 1998; Parés et al., 1999), and analysing the degree of anisotropy is a useful approach to illustrate changes in magnetic fabric in analogue models (Almqvist and Koyi, 2018; Schöfisch et al., 2020, 2022). For example, Schöfisch et al. (2022) showed that a decrease in degree of anisotropy occurs with decreasing distance to a fault~~, is observed (cf. Schöfisch et al., 2022)~~. Generally, AMS data from faults in shortened models show a lower degree of anisotropy compared to the data from areas away from faults. This is also the case in extensional settings, e.g., in Model I, where AMS data from the normal faults highlight this observation, but it is apparent that the change in degree of anisotropy is abrupt between normal faults and farther away from the faults (Fig. 3~~5~~). As discussed above (section 4.1), there is almost no penetrative strain developing within the footwall and hanging wall during extension. Normal faults develop from the onset of model extension (V1-2 in ~~Supplementary Material~~Supplement), illustrating a distinct difference between magnetic fabric away from faults and within/along faults. In contrast, in compressional regime, penetrative strain (and kinking) precedes thrusting, which needs more amount of model shortening before a thrust ~~fault~~ is created, compared to the "amount" of model extension that is needed for formation of a normal fault (V1-2 in Supplement~~ary Material~~). Penetrative strain is an important factor in changing the magnetic fabric and describes the transition of changes in magnetic fabric between the initial fabric to a thrust-induced fabric. In summary, unlike models II and III which show a gradual transition in degree of anisotropy across the models, Model I developed no gradual, but distinct change in degree of anisotropy with distance to a ~~thrust~~ fault ~~throughout the model~~ (comparing the slope of dashed lines from Model I with models II and III in Figs. 3a, b, and d). In addition, comparing models II and III, the gradient in degree of anisotropy becomes clearer with increasing bulk shortening (i.e., larger difference in Pj between faults and areas away from faults), which is ~~a~~ similar to observations ~~as~~ by Schöfisch et al. (2022). The decreasing gradient in the degree of anisotropy and, in general, the change in magnetic fabric with distance to faults (including principal axes orientation with confidence ellipses, shape and degree of anisotropy of magnetic ellipsoid) ~~with distance to faults~~ are distinct features that describe the difference between extensional and compressional tectonic regimes.

5 Advantages, limitations, and future perspectives of applying AMS to basin and basin inversion models

5.1 Depicting deformation and changes in deformation by AMS

Applying AMS allows visualising deformation in sandbox models (Almqvist and Koyi, 2018; Schöfisch et al., 2020, 2022). In the models of this study, the magnetic fabric also reflects deformation and the development of structures. In addition, this study reveals an overprint of magnetic fabric due to inversion, specifically, differences are monitored between extensional to compressional tectonic environments. Extension did not result in penetrative strain in the models, which is indicated by a persistent initial fabric throughout the hanging wall (i.e., graben) and footwalls of Model I and the sharp change in degree of anisotropy between normal faults and in areas away from the faults. In contrast, in shortened models (e.g., Schöfisch et al., 2022) or inverted models (models II and III of this study), shortening leads to development of penetrative strain in areas away from the faults. Consequently, the magnetic fabric is sensitive to strain changes in compressional regimes, but further studies are required for depicting extensional fabrics in more details in sandbox models.

As the models simulate brittle behaviour of upper crustal rocks without taking into account processes like crystal-plastic deformation, fluid migration, and recrystallisation of magnetic contributors (i.e., changes in magnetic mineralogy and development of sub-fabric), changes to the initial fabric in the models are solely related to grain reorientation. Such modelling setup and the combination of sandbox modelling with magnetic fabric analyses enables investigation, visualization, and highlighting the importance of grain reorientation in natural analogues.

5.2 Outlook: From limitations towards future models

As Eisenstadt and Sims (2005) and Deng et al. (2019) documented, there is no or very limited reactivation of pre-existing normal faults during inversion of such a model setup using loose sand above a ridged basal plate. In addition, an extensional fabric away from normal faults as observed in nature (e.g., Sagnotti et al., 1994; Mattei et al., 1997; Borradaile and Hamilton, 2004; Cifelli et al., 2005) is not displayed in these models. Therefore, it may be necessary to prepare similar experiments simulating the development of a basin and its inversion with higher complexity. For example, testing syn-tectonic basin sedimentation to create magnetic lineation in basin fill, or using different materials (e.g., wet clay) to produce extensional structures (e.g., roll-over anticlines; cf. Eisenstadt and Withjack, 1995; Eisenstadt and Sims, 2005). Moreover, different materials (Eisenstadt and Sims, 2005), oblique inversion (Nalpas et al., 1995; Brun and Nalpas, 1996; Dubois et al., 2002; Deng et al., 2019), or different modelling setups with viscous décollement (e.g., Roca et al, 2006; Del Ventisette et al., 2006 and references therein) lead to a reactivation of normal faults within the models. In such cases, investigating a magnetic fabric overprint due to fault reactivation is of great interest.

6 Conclusions

Three sandbox models were created to investigate the magnetic fabric in similar structures at different stages of basin inversion. Two distinct magnetic fabrics are observed in the extension model (Model I) prior to model inversion: an initial fabric away from the faults and normal fault-induceda fabric affected by normal faulting. In models which underwent With subsequent inversion (i.e., models II and III), the magnetic fabric is overprinted by layer-parallel ~~compaction~~ shortening (i.e., penetrative strain), developing a penetrative~~-~~ strain-induced fabric.

During inversion of models II and III, thrusts formed with different stages of thrust maturity. This different thrust maturity is also reflected in the magnetic fabric and shows a different degree of alignment of the magnetic foliation parallel to the thrust surface. Although, normal faults and thrusts ~~faults~~ showed a similar amount of displacement, their magnetic fabric differs from each other; thrusting is more efficient in aligning the magnetic fabric along the fault surface compared to normal faults~~ing~~. During inversion, the pre-existing normal faults define weak zones within a developing pop-up structure and ~~deform~~ passively rotate ~~during inversion~~ even though they show very little sign of inverted kinematics. This deformation is manifested by fault steepening that affects the magnetic fabric to become similar to a penetrative~~-~~ strain-induced fabric.

Irrespective of the orientation of principal axes, changes and gradients in the degree of anisotropy are identified depicting changes in the deformation pattern in the models. In extended models (Model I), the magnetic fabrics from different parts of the model are distinct from each other. However, the magnetic fabric in the inverted models shows an overprint from initial fabric towards penetrative strain-induced fabric, which develops into a fault-induced fabric along the thrusts.

Appendices

Additional figures with explanation for this study are summarized in the ~~Supporting Information~~Supplement ~~S1~~. ~~S1~~ The Supplement includes figures and tables analysing the narrowing of the basin during inversion (Fig. S1 ~~in S1~~) as well as an advanced analysis of the structure-to-sample-size ratio for AMS data at the faults (Fig. S2 ~~in S1~~). The Supplement includes also a figure comparing the mean of the principal axes with size of confidence ellipses for the areas away from faults (Fig. S3). Additionally, two gif-files show the structural development of models II and III as short videos (V1 and 2 in Supplement).

Data availability

The AMS data from the three models of this study are published at the open-source online data repository hosted by Mendeley Data (Schöfisch, 2022) with the following doi: 10.17632/bcxzzyrzj3.1~~-~~.

Authors contribution

TS: conceptualization, methodology, formal analysis, interpretation, writing – original draft, writing – review & editing, visualization; HK & BA: interpretation, writing – review & editing, supervision, funding acquisition

Competing interests

The authors declare no competing interests relevant to this study.

Acknowledgements

This study is supported by a research grant from the Swedish Research Council to HK and BA (VR, 2017–04519). Thanks are due to LKAB Minerals Luleå (Sweden) for providing the magnetite for modelling. Moreover, we thank ~~the editors~~Frank Zwaan for editorial handling and comments. We are grateful for the reviews by Michele Cooke, Kenneth Kodama, and Cristina García-Lasanta~~ of this special issue for this opportunity~~.

References

Allen, M., Poggiali, D., Whitaker, K., Marshall, T. R., van Langen, J., Kievit, R. A.: Raincloud plots: a multi-platform tool for robust data visualization [version 2; peer review: 2 approved]. Wellcome Open Res, **4**:63, https://doi.org/10.12688/wellcomeopenres.15191.2, 2021.

Almqvist, B.S.G. and Koyi, H.: Bulk strain in orogenic wedges based on insights from magnetic fabrics in sandbox models. Geology 46, 483–486. https://doi.org/10.1130/G39998.1, 2018.

Averbuch, O., Frizon de Lamotte, D., and Kissel, C.: Magnetic fabric as a structural indicator of the deformation path within a fold-thrust structure: a test case from the Corbières (NE Pyrenees, France). Journal of Structural Geology 14, 461–474. https://doi.org/10.1016/0191-8141(92)90106-7, 1992.

Bakhtari, H.R.., Frizon de Lamotte, D.., Aubourg, C., and Hassanzadeh, J.: Magnetic fabrics of Tertiary sandstones from the Arc of Fars (Eastern Zagros, Iran). Tectonophysics 284, 299–316. https://doi.org/PIIS0040-1951(97)00179-0, 1998.

Bonini, M., Sani, F., and Antonielli, B.: Basin inversion and contractional reactivation of inherited normal faults: A review based on previous and new experimental models. Tectonophysics 522–523, 55–88. https://doi.org/10.1016/j.tecto.2011.11.014, 2012.

Borradaile, G.J.: Magnetic susceptibility, petrofabrics and strain. Tectonophysics 156, 1–20. https://doi.org/10.1016/0040-1951(88)90279-X, 1988.

Borradaile, G. J.: Correlation of strain with anisotropy of magnetic susceptibility (AMS). Pure and Applied Geophysics PAGEOPH, 135(1), 15–29. https://doi.org/10.1007/BF00877006, 1991.

Borradaile, G.J. and Henry, B.: Tectonic applications of magnetic susceptibility and its anisotropy. Earth-Science Reviews 42, 49–93. https://doi.org/10.1016/S0012-8252(96)00044-X, 1997.

Borradaile, G. J., and Hamilton, T.: Magnetic fabrics may proxy as neotectonic stress trajectories, Polis rift, Cyprus, Tectonics, 23, TC1001, doi:10.1029/2002TC001434, 2004.

Borradaile, G.J. and Jackson, M.: Anisotropy of magnetic susceptibility (AMS); magnetic petrofabrics of deformed rocks Geol. Soc. Spec. Publ., 238, pp. 299-360, 2004.

Brun, J.-P. and Nalpas, T.: Graben inversion in nature and experiments, Tectonics, 15, 677–687, https://doi.org/10.1029/95TC03853, 1996.

Burmeister, K. C., Harrison, M. J., Marshak, S., Ferré, E. C., Bannister, R. A., and Kodama, K. P.: Comparison of Fry strain ellipse and AMS ellipsoid trends to tectonic fabric trends in very low-strain sandstone of the Appalachian fold-thrust belt. Journal of Structural Geology, 31(9), 1028–1038, 2009.

Burgin, H.B., Robion, P., and Amrouch, K.: Layer parallel stretching? Characterising magnetic and pore-fabric styles at a rifted continental margin: New insights from the Otway Ranges, Australia. Tectonophysics 815, 228975. https://doi.org/10.1016/j.tecto.2021.228975, 2021.

Cifelli, F., Mattei, M., Chadima, M., Hirt, A.M., and Hansen, A.: The origin of tectonic lineation in extensional basins: Combined neutron texture and magnetic analyses on “undeformed” clays. Earth and Planetary Science Letters 235, 62–78. https://doi.org/10.1016/j.epsl.2005.02.042, 2005.

De Lamotte Frizon, D., Souque, C., Grelaud, S., and Robion, P.: Early record of tectonic magnetic fabric during inversion of a sedimentary basin - short review and examples from the Corbières transfer zone (France). Bulletin de La Societe Geologique de France 173, 461–469. https://doi.org/10.2113/173.5.461, 2002.

Del Ventisette, C., Montanari, D., Sani, F., and Bonini, M.: Basin inversion and fault reactivation in laboratory experiments. Journal of Structural Geology 28, 2067–2083. https://doi.org/10.1016/j.jsg.2006.07.012, 2006.

Deng, H., Koyi, H.A., and Zhang, J.: Modelling oblique inversion of pre-existing grabens. Geological Society Special Publication 487, 263–290. https://doi.org/10.1144/SP487.5, 2019.

Dubois, A., Odonne, F., Massonnat, G., Lebourg, T., and Fabre, R.: Analogue modelling of fault reactivation: tectonic inversion and oblique remobilisation of grabens, J. Struct. Geol., 24, 1741-1752, https://doi.org/10.1016/S0191- 8141(01)00129-8, 2002.

Eisenstadt, G. and Withjack, M.O.: Estimating inversion: Results from clay models. Geological Society Special Publication 88, 119–136. https://doi.org/10.1144/GSL.SP.1995.088.01.08, 1995.

Eisenstadt, G. and Sims, D.: Evaluating sand and clay models: Do rheological differences matter? Journal of Structural Geology 27, 1399–1412. https://doi.org/10.1016/j.jsg.2005.04.010, 2005.

García-Lasanta, C., Oliva-Urcia, B., Román-Berdiel, T., Casas, A.M., and Hirt, A.M.: Understanding the Mesozoic kinematic evolution in the Cameros basin (Iberian Range, NE Spain) from magnetic subfabrics and mesostructures. Journal of Structural Geology, 66: 84-101. https://doi.org/10.1016/j. jsg.2014.05.013, 2014.

García-Lasanta, C., Oliva-Urcia, B., Román-Berdiel, T., Casas, A.M., Gil-Peña, I., Sánchez-Moya, Y., Sopeña, A., Hirt, A.M., and Mattei, M.: Evidence for the Permo-Triassic transten- sional rifting in the Iberian Range (NE Spain) according to magnetic fabrics results. Tectonophysics 651-652: 216-231. https://doi.org/10.1016/j.tecto.2015.03.023, 2015.

García-Lasanta, C., Izquierdo-llavall, E., Román-Berdiel, T.: Análisis de la fábrica magnética en modelos analógicos de arcillas (Magnetic fabric analysis in analogue models of clays). Geogaceta 61, 103–106, 2017

García-Lasanta, C., Oliva-Urcia, B., Casas-Sainz, A.M., Román-Berdiel, T., Izquierdo-Llavall, E., Soto, R., Calvín, P., Moussaid, B., El Ouardi, H., Kullberg, J.C., and Villalaín, J.J.: Inversion tectonics and magnetic fabrics in Mesozoic basins of the Western Tethys: A review. Tectonophysics 745, 1–23. https://doi.org/10.1016/j.tecto.2018.08.005, 2018.

Hirt, A.M., Lowrie, W., Clendenen, W.S., and Kligfield, R.: The correlation of magnetic anisotropy with strain in the Chelmsford Formation of the Sudbury Basin, Ontario. Tectonophysics 145, 177–189. https://doi.org/10.1016/0040-1951(88)90194-1, 1988.

Housen, B.A., Richter, C., van der Pluijm, B.A.: Composite magnetic anisotropy fabrics: experiments, numerical models and implications for the quantification of rock fabrics. Tectonophysics 220, 1–12. https://doi.org/10.1016/0040-1951(93)90219-A, 1993.

Hrouda, F. and Janák, F.: The changes in shape of the magnetic susceptibility ellipsoid during progressive metamorphism and deformation. Tectonophysics 34, 135–148. https://doi.org/10.1016/0040-1951(76)90181-5, 1976.

Hrouda, F.: Magnetic anisotropy of rocks and its application in geology and geophysics. Geophysical Surveys, 5(1), 37–82. https://doi.org/10.1007/BF01450244, 1982.

Jelínek, V.: The statistical theory of measuring anisotropy of magnetic susceptibility of rocks and its application. Geofyzika Brno, 87, 1977.

Jelinek, V.: Characterization of the magnetic fabric of rocks. Tectonophysics 79, T63–T67. https://doi.org/10.1016/0040-1951(81)90110-4, 1981.

Kligfield, R., Owens, and W.H., Lowrie, W.: Magnetic susceptibility anisotropy, strain, and progressive deformation in Permian sediments from the Maritime Alps (France). Earth and Planetary Science Letters 55, 181–189. https://doi.org/10.1016/0012-821X(81)90097-2, 1981.

Koyi, H.: Mode of internal deformation in sand wedges. Journal of Structural Geology 17, 293–300. https://doi.org/10.1016/0191-8141(94)00050-A, 1995.

Koyi, H.A., Sans, M., Teixell, A., and Zeyen, H.: The Significance of Penetrative Strain in the Restoration of Shortened Layers-Insights from Sand Models and the Spanish Pyrenees. Thrust Tectonics and Hydrocarbon Systems: AAPG Memoir. 82, 1–16, 2003.

Marcén, M., Román-Berdiel, T., Casas-Sainz, A.M., Soto, R., Oliva-Urcia, B., and Castro, J.: Strain variations in a seismogenic normal fault (Baza Sub-basin, Betic Chain): Insights from magnetic fabrics (AMS). Tectonophysics 765, 64–82. https://doi.org/10.1016/j.tecto.2019.05.014, 2019.

Mattei, M., Sagnotti, L., Faccena, C., and Funiciello, R.: Magnetic fabric of weakly deformed clay-rich sediments in the extensional tectonics. Tectonophysics 271, 107–122, 1997.

Mattei, M., Speranza, F., Argentieri, A., Rossetti, F., Sagnotti, L., and Funiciello, R.: Extensional tectonics in the Amantea basin (Calabria, Italy): A comparison between structural and magnetic anisotropy data. Tectonophysics 307, 33–49. https://doi.org/10.1016/S0040-1951(99)00117-1, 1999.

Mulugeta, G. and Koyi, H.: Episodic accretion and strain partitioning in a model sand wedge. Tectonophysics 202, 319–333. https://doi.org/10.1016/0040-1951(92)90117-O, 1992.

Nalpas, T., Le Douaran, S., Brun, J.-P., Unternehr, P., and Richert, J.-P.: Inversion of the Broad Fourteens Basin (offshore Netherlands), a small-scale model investigation, Sediment. Geol., 95, 237–250, https://doi.org/10.1016/0037-0738(94)00113-9, 1995.

Oliva-Urcia, B., Casas, A.M., Soto, R., Villalaín, J.J., and Kodama, K.: A transtensional basin model for the Organyà basin (central southern Pyrenees) based on magnetic fabric and brittle structures. Geophysical Journal International, 184 (1): 111-130. https://doi.org/10.1111/j.1365-246X.2010.04865.x, 2010.

Oliva-Urcia, B., Román-Berdiel, T., Casas, A.M., Bogalo, M.F., Osácar, M.C., and García-Lasanta, C.: Transition from extensional to compressional magnetic fabrics in the cretaceous Cabuérniga basin (North Spain). Journal of Structural Geol- ogy, 46: 220-234. https://doi.org/10.1016/j.jsg.2012.09.001, 2013.

Oliva-Urcia, B., Casas, A.M., Moussaid, B., Villalaín, J.J., El Ouardi, H., Soto, R., Torres-López, S., and Román-Berdiel, T.: Tectonic fabrics vs. mineralogical artifacts in AMS analysis: a case study of the Western Morocco extensional Triassic basins. Journal of Geodynamics, 94-95: 13-33. https://doi.org/10.1016/j.jog.2016.01.004, 2016.

Parés, J.M., Van der Pluijm, B.A., and Dinarès-Turell, J.: Evolution of magnetic fabrics during incipient deformation of mudrocks (Pyrenees, northern Spain). Tectonophysics 307, 1–14. https://doi.org/10.1016/S0040-1951(99)00115-8, 1999.

Parés, J.M., and Van Der Pluijm, B.A.: Evaluating magnetic lineations (AMS) in deformed rocks. Tectonophysics 350, 283–298. https://doi.org/10.1016/S0040-1951(02)00119-1, 2002.

Parés, J.M.: Sixty years of anisotropy of magnetic susceptibility in deformed sedimentary rocks. Frontiers in Earth Science 3, 4. https://doi.org/10.3389/feart.2015.00004, 2015.

Roca, E., Sans, M., and Koyi, H.A.: Polyphase deformation of diapiric areas in models and in the eastern Prebetics (Spain). AAPG Bulletin, 90, 115–136. https://doi.org/10.1306/07260504096, 2006.

Rochette, P., Jackson, M., Aubourg, C.: Rock magnetism and the interpretation of anisotropy of magnetic susceptibility. Reviews of Geophysics 30, 209. https://doi.org/10.1029/92RG00733, 1992.

Sagnotti, L., Faccenna, C., Funiciello, R., and Mattei, M.: Magnetic fabric and structural setting of Plio-Pleistocene clayey units in an extensional regime: the Tyrrhenian margin of central Italy. Journal of Structural Geology 16, 1243–1257. https://doi.org/10.1016/0191-8141(94)90067-1, 1994.

Sassi, W., Colletta, B., Balé, P., Paquereau, T.:Modelling of structural complexity in sedimentary basins: The role of pre-existing faults in thrust tectonics. Tectonophysics 226, 97–112. https://doi.org/10.1016/0040-1951(93)90113-X, 1993

Schöfisch, T., Koyi, H., and Almqvist, B.: Influence of décollement friction on anisotropy of magnetic susceptibility in a fold-and-thrust belt model. Journal of Structural Geology 144. https://doi.org/10.1016/j.jsg.2020.104274, 2020.

Schöfisch, T., Koyi, H., and Almqvist, B.: Magnetic Fabric Signature Within a Thrust Imbricate; an Analog Modeling Approach. Tectonics 41, 1–18. https://doi.org/10.1029/2021TC007054, 2022.

Schöfisch, T.: “Magnetic Fabric Distribution in inverted Basin Sandbox Models”, Mendeley Data, V1, doi: 10.17632/bcxzzyrzj3.1, 2022

Soto, R., Casas-Sainz, A.M., Villalaín, J.J., and Oliva-Urcia, B.: Mesozoic extension in the Basque-Cantabrian basin (N Spain). Contributions from AMS and brittle mesostructures. Tectonophysics, 445: 373-394. https://doi.org/10.1016/j.tecto.2007.09.007, 2007

Soto, R., Casas-Sainz, A.M., Villalaín, J.J., Gil-Imaz, A., Fernández-González, G., Del Río, P., Calvo, M., and Mochales, T.: Characterizing the Mesozoic extension direction in the northern Iberian plate margin by anisotropy of magnetic susceptibility (AMS). Journal of the Geological Society, 165: 1007-1018. https://doi.org/10.1144/0016-76492007-163, 2008.

Soto, R., Kullberg, J.C., Oliva-Urcia, B., Casas-Sainz, A.M., and Villalaín, J.J.: Switch of Mesozoic extensional tectonic style in the Lusitanian basin (Portugal): Insights from mag- netic fabrics. Tectonophysics, 536-537: 122-135. https://doi. org/10.1016/j.tecto.2012.03.010, 2012.

Soto, R., Larrasoaña, J.C., Beamud, E., and Garcés, M.: Early-Middle Miocene subtle compressional deformation in the Ebro foreland basin (northern Spain); insights from magnetic fabrics. Comptes Rendus Geoscience, 348(3-4): 213-223. https://doi.org/10.1016/j.crte.2015.10.009, 2016.

Tong, H., Koyi, H., Huang, S., and Zhao, H.: The effect of multiple pre-existing weaknesses on formation and evolution of faults in extended sandbox models. Tectonophysics 626, 197–212. https://doi.org/10.1016/j.tecto.2014.04.046, 2014.